Available online at www.sciencedirect.com

ScienceDirect

Procedia Structural Integrity 2 (2016) 3772–3781

Structural Integrity Procedia

www.elsevier.com/locate/procedia

21st European Conference on Fracture, ECF21, 20-24 June 2016, Catania, Italy

Fatigue and Fracture behaviour of AZ31b Mg alloy plastically deformed by Constrained Groove Pressing in the Presence of Overloads

Enrico Salvati[a], Hongjia Zhang[a], Kai Soon Fong[b], Robert J.H. Paynter[a], Xu Song[b], Alexander M. Korsunsky[a]

[a]*Department of Engineering Science, University of Oxford, Parks Road, Oxford, OX13PJ, United Kingdom*
[b]*Forming Technology Group, Singapore Institute of Manufacturing Technology, Singapore*

Abstract

Within the class of lightweight metallic materials, magnesium alloys are gaining popularity mainly thanks to abundant supply and high specific strength. A weakness of Mg alloys is their poor formability at room temperature. For this reason, in recent years thermo-mechanical treatments have often been sought that would improve this aspect. One particular way towards the combination of better formability (ductility) and strength is through grain refinement by means of Constrained Groove Pressing (CGP). The use of a pair of matching dice having groove-like geometry, coupled with controlled process temperature, allows promoting microstructural refinement and achieving sub-micron grain size in the processed plates.

The purpose of the present study was to characterise the resulting fine-grained material in plate form in terms its fatigue fracture behaviour. Compact tension samples were machined and subjected to cyclic tensile loading to monitor fracture propagation and extract their Fatigue Crack Growth Rate (FCGR) behaviour as a function of the applied crack tip Stress Intensity Factor range. Firstly, as a reference sample an as-received material plate was tested at the loading ratio R=0.1. Subsequently, CGP-processed fine-grained material was tested at R=0.1 and R=0.7, and subjected to anomalous load that included overload (50% increase in the maximum load) and, in the specific case of R=0.1, underload (reversal of the sign of minimum load from tension to compression).

These studies provided the critically needed input for the development of new approaches to the evaluation of the apparent fracture resistance of the material processed by CGP under variable amplitude loading (i.e. overload and underload) essential for accurate fatigue life prediction for a broad variety of applications. By combining the Walker model accounting for the mean stress effect and a modified Wheeler model for crack growth retardation due to the application of a single overload, a new predictive approach was formulated.

Peer-review under responsibility of the Scientific Committee of ECF21.

Keywords: Mg Alloy, SPD, fatigue, fracture, Walker, Wheeler, Overload, Underload

Copyright © 2016 The Authors. Published by Elsevier B.V. This is an open access article under the CC BY-NC-ND license (http://creativecommons.org/licenses/by-nc-nd/4.0/).
Peer review under responsibility of the Scientific Committee of ECF21.
10.1016/j.prostr.2016.06.469

1. Introduction

The ultimate goal of engineering with materials is to create structures that are both strong and lightweight. Magnesium alloys are gaining attention due to their exceptional specific stiffness, strength, corrosion properties and machinability, Avedesian (1999). In fact, Mg alloys are the lightest structural metals and have mechanical properties comparable to those of other lightweight alloys (e.g. Al). Furthermore, Mg alloys may show an outstanding ability to absorb energy, making them the ideal choice for applications where high damping capacity is required.

Mg alloys show good castability, making them suitable for the fabrication of complex shape mechanical components. However, a weakness lies in the poor formability of Mg alloys at room temperature. For this reason in recent years considerable research effort has been directed at developing mechanical and thermo-mechanical treatments to improve this property, He (2016) and Song (2015). The common approach of all these processes is aimed at grain refinement by plastic deformation and the removal or reduction of pronounced texture arising from the production of Mg sheets. The effect of grain refinement is the reduction of the twinning activity in the first stages of deformation with a consequent change in the predominant slip mechanism to dislocation cross-slip at non-basal planes, Koike al. (2003).

Among the several ways to induce grain refinement severe plastic deformation (SPD) treatments, Hana (2016) and Chen (2016), Constrained Groove Pressing (CGP) is one such method that produces sub-micron grain structure and confers substantially better formability properties on the material. In addition, such process generates practically uniform grain size microstructure, Yang (2006). The process is accomplished through the use of two dies having groove-like geometry, coupled with controlled temperature schedule. The parent Mg plate is then placed between the two dies and plastically deformed. Usually, several passes are required in order to obtain a uniformly distributed grain size.

The aim of this study is the characterization of fatigue resistance of a fine-grained material produced by a specific CGP sequence. Parent material was first subjected to four passes at the same sheet orientation and subsequently deformed with further four passes in the direction orthogonal to the first. The process details, and further information regarding the microstructure, texture and residual stress estimation are provided in another publication, Fong (2015). This sample condition is referred to as “DA”. Compact Tension (CT) samples were machined from the treated sheets and subjected to cyclic loading to determine the Fatigue Crack Growth Rate (FCGR). Tests were performed under loading control at two different load ratios (R=0.1 and R=0.7) in order to evaluate the mean stress sensitivity. With the goal of assessing the material response at the occurrence of the anomalous loads during a constant amplitude fatigue test, two experiments were performed with overloads (OL) applied during the crack propagation under baseline load ratio test conditions. Beside this, the Fatigue Crack Growth Rate (FCGR) response at the occurrence of an Underload (UL) was also studied in the case of R=0.1. Furthermore, for comparison the parent material that had not been subjected to CGP was also tested at R=0.1 with the purpose of quantifying the baseline material’s fatigue resistance properties.

In the first instance, the constant amplitude loading results were modelled using a Walker model, Walker (1970). In this way, the FCGR for both the loading ratios could be represented as function of a unique equivalent Stress Intensity Factor (eSIF) which accounts the material sensitivity to the mean stress. Wheeler model, Wheeler (1972), was then introduced for the modelling of the FCGR response at the OL occurrence. Recently, some modified versions of the Wheeler model were proposed in order to capture also the gradual reduction in FCGR after the OL until it reaches its minimum (delay part), Yuen (2006) and Mehrzadi (2013). The modified Wheeler model proposed by Yuen was implemented for the two loading ratios; this could be done incorporating the eSIF calculated through Walker.

The outcomes of the experimental and modelling parts are discussed below.

2. Material description and fatigue test

The material tested in the present manuscript is a Magnesium alloy AZ31b subjected to CGP severe plastic deformation. As result of the treatment, a refined grain size in the micron range is generated, and it displays an increase in tensile strength with respect to the base heat treatment. The resulting combination of properties is

characterised by the yield stress of $\sigma_y \approx 260$MPa, yield strain of ~0.6%, and the grain size distributed in the range from <1 μ m to 5 μ m maximum.

A 2mm-thick miniature Compact Tension (CT) specimen (35mm) was machined from the treated plate for fatigue testing. For the details of the sample geometry the reader is referred to a previous publication, Salvati (2016). A servo-hydraulic fatigue rig, capable of applying cyclic loading up to 20kN, was used for performing cyclic loading (fatigue). The baseline constant amplitude fatigue loading was performed at the frequency of 7Hz, while, the crack length was monitored using an optical microscope system providing images at 1024x1024pixels of resolution and pixel size of around 1μm. This allowed precise determination of the crack length and evaluation of fatigue crack growth rate (FCGR). The fatigue test setup is depicted in Fig.1(a).

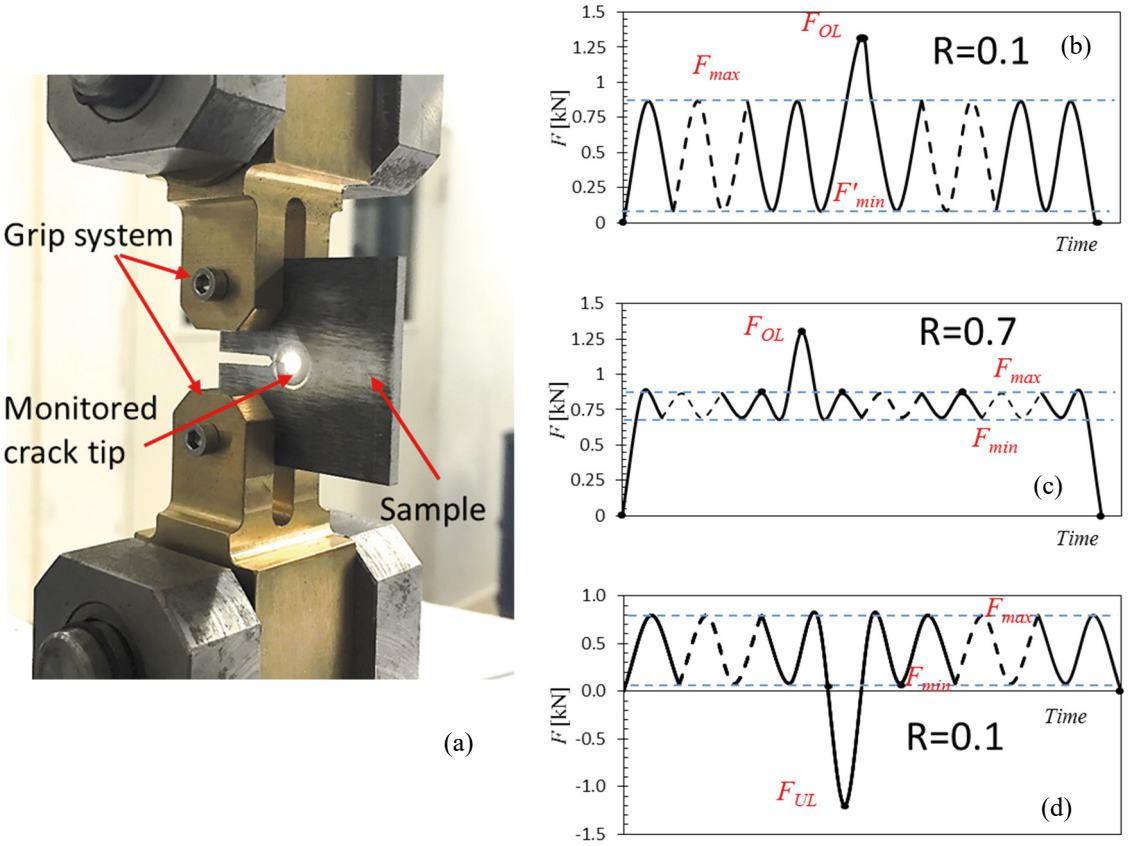

Fig. 1. (a) Test setup arrangement; (b-c-d) fatigue loading history.

The sample denoted DA1 was cyclically loaded at constant amplitude as shown in Fig.1b (without OL). The load range was between the maximum load of F_{min}=0.87kN and minimum load of F_{max}=0.087kN, i.e. the load ratio R=0.1. Additional experiments were conducted on two samples designated DA2 and DA3 with a different load ratio R=0.7, but maintaining the maximum load unchanged, with the maximum and minimum loads of 0.87kN and 0.69kN, respectively.

Sample DA UL1 was tested at the same fatigue baseline as sample DA1, but subjected to a single underload (UL) when the crack length reached 4.5mm. A single UL of magnitude FUL=-1.2kN was applied in accordance with loading sequence shown in Fig.1d.

For both load ratios of R=0.1 and R=0.7, a single anomalous OL was applied when the crack had reached the length of 9mm. The magnitude of the OL was such that the ratio between the OL and the maximum cyclic load was

ROL=1.5, therefore FOL=1.3KN. For R=0.1 and R=0.7 the samples subjected to OL were designated respectively DA OL1 and DA OL2. The two fatigue loading sequences are illustrated in Figs. 1b and 1c.

An additional sample (Parent material) was tested under the same loading conditions as sample DA1 with the purpose of obtaining the baseline fatigue crack propagation rate data for the same material before CGP processing.

3. Fatigue test results and discussion

The analysis of the experimental data (i.e. number of cycles and crack length) allowed the construction of FCGR curves vs. driving force for crack growth. The calculation of the SIF for the micro-CT sample was conducted by using the convenient formulation proposed by Murakami (1987). Fig.2 shows all experimental points obtained in this fatigue testing campaign.

The first observation that can be drawn from these experimental outcomes is in regards to the fatigue performance of the processed material compared to the un-processed material at R=0.1. The plastically deformed material showed the same fatigue resistance as the parent material: the experimental points overlap, and no noticeable systematic differences are apparent. This observation provides the evidence that severe plastic deformation treatment applied to Mg alloy sheet material did not alter its fracture toughness and fatigue strength. This is a very important observation, since the most commonly noted result of SPD treatments is the improvement of tensile strength that often is accompanied by a reduction in the fatigue and fracture properties. In the present case it can be concluded that processing did not compromise the fatigue crack propagation resistance. The SIF range where the FCGR can be represented by the Paris law varies from around 12.7 MPa √m up to around 32 MPa √m for low loading ratio R=0.1. This material turned out to have better fatigue crack resistance properties compared to the as-extruded AZ31B Mg alloy material found in literature, Hongxia (2011).

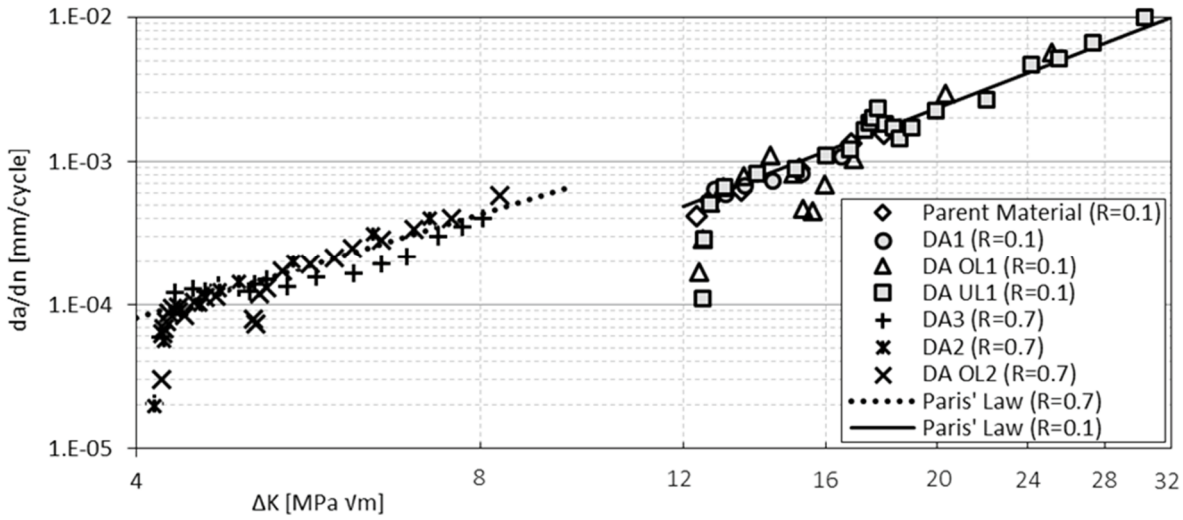

Fig. 2. FCGR results for the two loading conditions (R=0.1 and R=0.7).

Fatigue tests run at higher loading ratio R=0.7 highlighted the influence of the mean load. In fact, at low load ratio (R=0.1) the fatigue threshold is ~12.4 MPa √m, whereas for R=0.7 this value drops to ~4.2 MPa √m. Such influence can be quantified in terms of the sensitivity coefficient in the Walker model, as shown in the next section.

The two sets of data can be described using Paris law:

$$\frac{da}{dN} = C\,\Delta K^{m} \tag{1}$$

The fitting of the experimental data with the above equation (1) within the Paris law regime of propagation provides further information regarding the propagation behaviour. The fitted coefficients are reported in Table 1.

Table 1. Paris coefficients for the two load ratios.

Loading Ratio R	C [m/(cycle MPa √m)]	m
0.1	2.34×10^{-10}	3.07
0.7	2.85×10^{-9}	2.41

The coefficient m indicates the slope of the FCGR vs SIF range curve. The higher load ratio shows a slightly steeper curve. Nevertheless, these two values can be considered very close.

The OL gave rise to crack retardation for both loading conditions, as expected. The FCGR retardation for R=0.1 persisted longer than for R=0.7. This effect is discussed later along with the predictive modelling approach to the description of crack retardation. Furthermore, a crack arrest occurred at R=0.7 after the OL and further 2000 cycles were required in order to re-nucleate the crack before further propagation.

The UL produced a brief spell of crack acceleration, as shown by the square markers in Fig.2. Given its short lasting effect, it can be stated that overall UL has a less significant effect in terms of the perturbation of FCGR compared to the OL effect.

4. The Walker model and its integration with the modified Wheeler model

4.1. The Walker model

Fatigue crack growth behaviour description that accounts for the mean stress effect and thus for the change in the load ratio can be put forward on the basis of the Walker model. This method was firstly adopted in the context of stress-life curves, Dowling (2009), Livieri (2015), Onn (2015), and subsequently successfully applied in the context of fracture mechanics, Cheng (1997) and Duran (2015). In particular, regarding its application to fracture mechanics, the effect of the load ratio (for $R\geq0$) can be incorporated by introducing a further parameter γ that denotes the material mean stress sensitivity. Such parameter is integrated in the original Paris' law formulation, and therefore its validity is confined to the Paris' regime.

The description of any combination of maximum SIF K_{max} and minimum SIF K_{min} can be expressed in terms of the load ratio R by introducing an equivalent parameter ΔK_{eq} to describe the FCGR for any combination. The equivalent SIF range ΔK_{eq} defined by Walker is the following:

$$\Delta K_{eq} = K_{max}(1-R)^{\gamma} \tag{2}$$

Here γ is the measure of material-specific FCGR sensitivity to the mean stress that ranges between 0 and 1. It is worth noting that the range of SIF can be expressed as function the loading ratio: $\Delta K = K_{max}/(1-R)$. Taking advantage of this formulation, we adopt a way more convenient for the present purpose to express equation (2) directly in terms of the SIF range and the load ratio R:

$$\Delta K_{eq} = \Delta K(1-R)^{\gamma-1} \tag{3}$$

In the Walker model, the parameters that describe the FCGR behaviour of the specific case R=0 according to the Paris' law C and m, are used as reference parameters and are then fixed. Therefore we can express those values, through the Paris' formulation:

$$\left(\frac{da}{dN}\right)_{R=0} = C_0\,\Delta K^{m_w} \tag{4}$$

Here C_0 and m_w are the material constants, and subscript w refers to the use of the Walker parameter. Based on the above, expression for the general case is obtained by substituting equation (3) into (4), replacing ΔK with ΔK_{eq}:

$$\left(\frac{da}{dN}\right)_w = C_0 \left[\Delta K_{eq}\right]^{m_w} = C_0 \left[\Delta K (1-R)^{\gamma-1}\right]^{m_w} \tag{5}$$

This formulation provides a description of

$$log\left(\frac{da}{dN}\right)_w = log(C_0) + m_w\, log(\Delta K) + m_w(\gamma-1)\, log(1-R) \tag{6}$$

Considering solely the set of experimental data presented here in the crack propagation regime unaffected by the OL, linear regression can be applied, leading to the graphical representation of the outcomes in Figure 3.

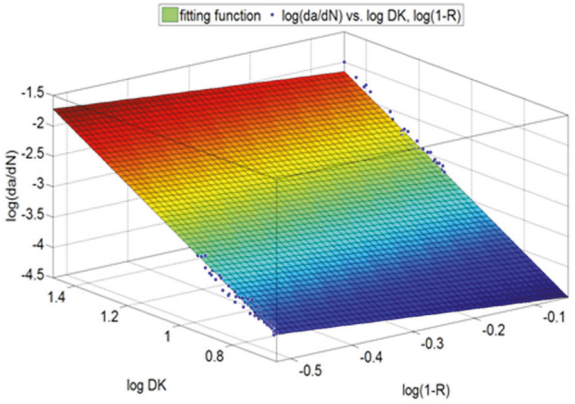

Fig. 3. Three-dimensional representation of the fitting function to the experimental data.

It is clear from Fig.3 that the fitting plane captures the trends for both sets of data. This is also confirmed by the low value of residuals. The outcomes of the outlined fitting procedure are hence the Walker parameters: $\gamma = 0.666$, $C_0 = 5.25 \times 10^{-10} m/(cycle\ MPa\sqrt{m})$, $m_w = 2.75$.

The value of γ denotes the relatively high sensitivity that the material has to the mean stress.

4.2. The modified Wheeler model

With some simplifications adopted, the fatigue crack growth retardation due to an overload can be predicted using the Wheeler model. Wheeler assumes that the retardation occurs immediately after the anomalous load application and the extension in which the retardation persist coincides with the plastic zone generated by the overload.

Such retardation is predicted thanks to the introduction of the retardation coefficient $\emptyset_R$ in the Paris' law formulation as follows:

$$\frac{da}{dN} = \emptyset_R \left(\frac{da}{dN}\right)_{CAL} \tag{7}$$

$$\text{where: } \emptyset_R = \begin{cases} \left[\dfrac{r_{p,i}}{a_{OL} + r_{p,OL} - a_i}\right]^{m_{wh}} & \text{if: } \quad a_i + r_{p,i} < a_{OL} + r_{p,OL} \\ 1 & \text{if: } \quad a_i + r_{p,i} > a_{OL} + r_{p,OL} \end{cases} \tag{8}$$

The retardation coefficient $\emptyset_R$ is a function of the overload effective plastic radius $r_{p,OL}$, the current cyclic plastic radius $r_{p,i}$ (i.e. generated at each cycle by the baseline load after OL), the current crack length a_i and the crack length at which the OL is applied a_{OL}. The magnitude of retardation is controlled by the shaping exponent m_{wh} and is obtained by matching to the experimental data.

Nevertheless, Walker model is not able to predict the retardation delay, i.e. the potential presence of initial short crack acceleration and overloads interaction. As mentioned earlier, some studies have attempted to include these effects in a Wheeler-based model. Concerning the purpose of the present work, we decided to introduce the delay correction to the original Wheeler model. In this way, the gradual FCGR deceleration occurring past the OL could be modelled. This task could be accomplished introducing the delay parameter $\emptyset_D$ as described by Yuen (2006). Therefore, the formulation of the FCGR becomes:

$$\frac{da}{dN} = \emptyset_R \emptyset_D \left(\frac{da}{dN}\right)_{CAL} \tag{9}$$

Similarly to the retardation coefficient, the delay coefficient can be expressed as:

$$where: \emptyset_D = \begin{cases} \left[\dfrac{a_{OL} + r_{d,OL} - a_i}{r_{d,i}}\right]^{m_{mod}} & \text{if: } \quad a_i + r_{d,i} < a_{OL} + r_{d,OL} \\ 1 & \text{if: } \quad a_{OL} + r_{d,OL} > a_i + r_{d,i} \end{cases} \tag{10}$$

Here $r_{d,OL}$ is the size of the OL effective delay, $r_{d,i}$ is the size of the current effective delay zone and m_{mod} is the shaping exponent for the modified model.

Several equations have been proposed in the past aimed at estimating the plastic radius that should be coincident with the effective plastic radius. The extension of the plastic zone is known to be function of the Stress Intensity factor *K* and the yield strength of the material σ_y and is usually defined as:

$$r_p = \alpha \left(\frac{K_{max}}{\sigma_y}\right)^2 \tag{11}$$

Here α is the plastic zone coefficient that is mainly dependent on the sample thickness, maximum SIF and mechanical properties. From one of the most popular and simple formulation proposed by Irwin (1968) to the more recent expressions based on Finite Element modelling, Xiaoping (2008), many attempts have been made in order to evaluate this coefficient. Nevertheless, in practical use it is observed that the extent of the plastic zone does not correspond to the real retardation length (effective plastic zone). Therefore the best fitting with the experimental data provides the most reliable value, Yuen (2006). In this work, we followed the fitting procedure firstly introduced by Yuen where the plastic zone coefficient is calculated by:

$$a_r = r_{p,OL} - r_{p,r} = \alpha_r \left[\left(\frac{K_{OL}}{\sigma_y}\right)^2 - \left(\frac{K_r}{\sigma_y}\right)^2\right] \tag{12}$$

Thus, the total retardation crack length a_r is thought of as the difference between the effective plastic zone induced by the OL and the plastic zone induced by the last cycle immediately before the crack outgrows the affected region.

Similarly to the plastic zone which corresponds to the retardation extension, Yuen (2006) proposed the definition of the delay zone r_d. This coefficient in turn can be evaluated in the same way as shown in (13):

$$a_d = r_{d,OL} - r_{d,d} = \alpha_d \left[\left(\frac{K_{OL}}{\sigma_y}\right)^2 - \left(\frac{K_d}{\sigma_y}\right)^2\right] \tag{13}$$

Here $r_{d,d}$ and K_d are respectively the delay radius and the stress intensity factor when the crack propagates to the length of $a_{OL} + a_d$.

4.3. The Walker-Wheeler models integration

So far, the model we described is able to predict fatigue crack retardation at low loading ratio R. Since we want to extend this model further to high values of R, we propose to assemble the two models described above. This can be readily implemented considering the Wheeler model that uses the eSIF evaluated according to Walker. In this way any combination of load ratio and overload retardation can be modelled by replacing the FCGR evaluated by Walker (5) into the Wheeler retardation model (9). The final formulation becomes:

$$\frac{da}{dN} = \emptyset_R \emptyset_D \left[C_0 \left[\Delta K_{eq}\right]^{m_w}\right] = \emptyset_R \emptyset_D [C_0 \, [\Delta K (1-R)^{\gamma-1}]^{m_w}] \tag{14}$$

4.4. Results and Discussion

The proposed calculation framework for the modelling of the overload effect on the FCGR retardation was applied to the experimental data.

It is noted that regarding for the load ratio R=0.7, the crack arrested its propagation right after the OL, and no delay part was detected. Therefore, since the proposed model is not able to account for the arrest effect, for this specific case we did not attempt the modelling of the delay part of propagation after OL. On the other hand, in the case of R=0.1, the delay was observed and the full modelling procedure was implemented.

The matching process aimed at the evaluation of the model's coefficients produced the values showed in Table 2.

Table 2. Wheeler model coefficients.

R	m_{wh}	m_{mod}	α_r	α_d
0.1	1.25	1.95	0.742	0.199
0.7	0.40	-	0.218	-

The results of the Walker-Wheeler model application are graphically represented on the Paris diagram of equivalent SIF evaluated using Walker ΔK_{eq} against the FCGR $\frac{da}{dN}$, as shown in Fig.4. Overall, the application of the model provided satisfactory matching with the experimental data. Fig. illustrates that good agreement is achieved with a very low level of scatter and deviation.

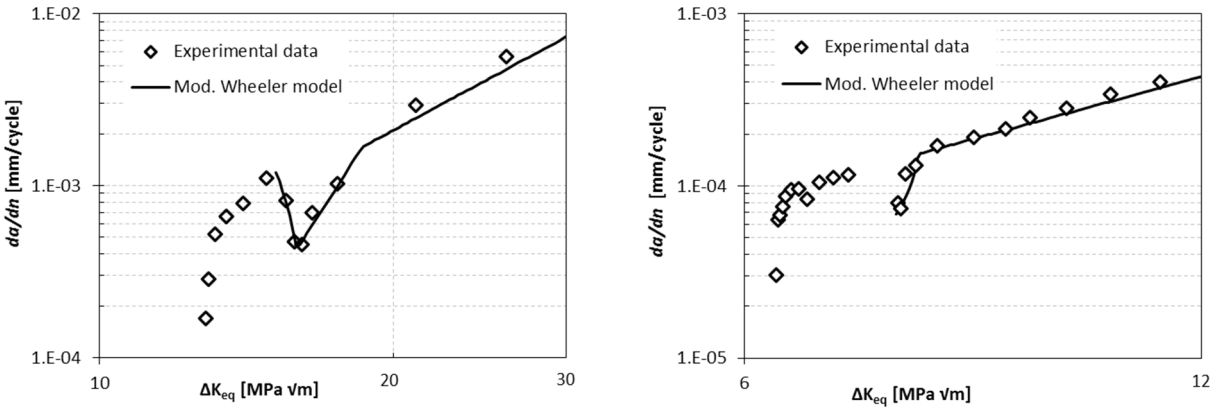

Fig. 4. Modelled and experimental FCGR (a) Loading Ratio R=0.1 (b) Loading Ratio R=0.7.

We note that the values of the shaping exponent and the plastic zone coefficients differ in the two loading conditions. It is important to make this observation because the Wheeler model is built on the correlation between the plastic radius and the extent of the OL effect. This means that theoretically the two loading cases should show the same values, since the OL load level is the same. However, at the high loading ratio R the effective plastic radius

produced by the OL ($r_{p,OL}$) resulted to be less than one third smaller of the one at R=0.1. This leads us to think that different crack propagation and retardation mechanisms were operating in the two experiments. The two predominant causes of crack retardation are thought to be the plasticity induced crack closure and the presence of compressive residual stress ahead of the crack tip. In the particular case of very high loading ratio it has been remarked that the crack closure effect may not be present, Borrego (2003). The absence of crack closure after OL at R=0.7 provides an explanation of the difference between the two sets of results. Indeed, the model does not account for the two mechanisms separately, and the reduction of retardation due to high R cannot be considered in the model.

Once the Walker-Wheeler model coefficients have been calibrated, the newly formulated model can be used for the prediction of the OL effect on crack retardation at different load ratios and different OL levels. It is important to note that the coefficients evaluate for the Wheeler model need to be interpolated for obtaining a more reliable prediction at load ratios R that differ from the two analysed in this paper (i.e. R=0.1 and R=0.7). Obviously, further experimental points may help improve the statistical coverage and thus the reliability of the model, especially at loading conditions largely different from the two treated here.

5. Conclusion

The fatigue crack growth response of Magnesium alloy AZ31b subjected to CGP severe plastic deformation was extensively analysed in the present work. The FCGR comparison between the parent material and the CGP-processed material, both tested at the load ratio R=0.1 revealed no substantial differences. This indicates that no significant alteration occurred in the fatigue resistance with the application of the thermo-mechanical treatment. At the load ratio of R=0.1 the fatigue crack growth threshold was found to be $\Delta K_{th,R=0.1} \approx 12MPa\sqrt{m}$. Further tests at the loading ratio R=0.7 showed a reduced threshold of $\Delta K_{th,R=0.7} \approx 4.2MPa\sqrt{m}$. The fitting of experimental data with the Paris coefficients showed nearly the same FCGR curve slope for the two loading ratios.

Fatigue tests conducted with the introduction of an OL revealed the retardation behaviour of the material. In both fatigue baseline situations crack propagation showed retardation, and in the case of R=0.7 the crack was even arrested for 2000 cycles. A single test was also performed where an UL was applied at the R=0.1 baseline fatigue test. This showed crack acceleration with a quick restoration of the original steady-state FCGR. However, the effect that UL had on the modification of FCGR was less prominent than the OL.

The fatigue crack growth behaviour was modelled using the combination of the Walker model that accounts for material sensitivity to mean stress, and a modified Wheeler model for the crack retardation prediction of crack delay after the occurrence of OL. This model can be used for the prediction of FCGR at different load and overload ratios upon the interpolation of the fitted coefficients.

To evaluate the physical meaning and the values of the model parameters, further investigations are required to understand the precise role of crack closure and residual stress in crack retardation. Additionally, further studies may be addressed at the description of the crack arrest behaviour in the present model, to endow this modelling approach with this capability.

Acknowledgements

AMK acknowledges funding received by MBLEM through EU FP7 project iSTRESS (604646).

References

Avedesian M.M., Baker H., 1999. Magnesium and Magnesium Alloys, M., ASM International, Materials Park.

Borrego L.P., Ferreira J.M., Pinho da Cruz J.M., Costa J.M., 2003. Evaluation of overload effects on fatigue crack growth and closure. Eng. Fracture Mechanics 70,1379–1397

Chen W., Zhang W., Qiao Y., Miao Q., Wang E., 2016. Enhanced ductility in high-strength fine-grained magnesium and magnesium alloy sheets processed via multi-pass rolling with lowered temperature. Journal of Alloys and Compounds 665, 13-20.

Dowling N. E., Calhoun C.A., Arcari A., 2009. Mean stress effects in stress-life fatigue and the Walker equation. Fatigue and Fracture of Engineering Materials and Structures. 32(3), 163-179

Duran J. A. R., Boloy R. M., Leoni R. R., 2015. Some remarks on the engineering application of the fatigue crack growth approach under nonzero mean loads. Front. Mech. Eng., 10(3), 255–262.

Fong S., Atsushi D., Jen T.M., Chua B.W., 2015., Effect of Deformation and Temperature Paths in Severe Plastic Deformation Using Groove Pressing on Microstructure, Texture, and Mechanical Properties of AZ31-O. Journal of Manufacturing Science and Engineering, 137, 051004-1.

Hana T., Huanga G., Wanga Y., Wanga G., Zhaoa Y., Pan F., 2016. Enhanced mechanical properties of AZ31 magnesium alloy sheets by continuous bending process after V-bending. Progress in Natural Science: Materials International 26, 97–102.

He W., Zeng Q., Yu H., Xin Y., Luan B., Liu Q. 2016. Improving the room temperature stretch formability of a Mg alloy thin sheet by pre-twinning. Materials Science & Engineering A 655, 1–8.

Hongxia Z., Zhifeng Y., Wenxian W., Peiyang L., Hongzhi L., Yinghui W., 2011. As-extruded AZ31B Magnesium Alloy Fatigue Crack Propagation Behavior. Journal Wuhan University of Technology, Materials Science Edition, 26(6), 1114-1120,

Irwin G., 1968. Linear Fracture Mechanics, fracture transition, and fracture control. Eng. Fract. Mech. 1, 214-57

Koike J., Kobayashi T., Mukai T., Watanabe H., Suzuki M., Maruyama K., et al., The activity of non-basal slip systems and dynamic recovery at room temperature in fine-grained AZ31B magnesium alloys, Acta Materialia, 51, 2055-2065.

Livieri P., Salvati E., Tovo R., 2016. A non-linear model for the fatigue assessment of notched components under fatigue loadings. International Journal of Fatigue, 82(3), 624-633.

Mehrzadi M., Taheri F., 2013. A material sensitive modified Wheeler model for predicting the retardation in fatigue response of AM60B due to an overload. Int. Journal of Fatigue 55, 220-229

Murakami Y.. 1987. Stress Intensity Factors Handboo, Pergamon Press 2.

Onn I. H., Ahmad N., Tamin M. N. 2015. Fatigue characteristics of dual-phase steel sheets. Journal of Mechanical Science and Technology 29 (1), 51-57.

Salvati E., O'Connor S., Sui T., Nowell D., Korsunsky A.M., 2016. A Study of Overload Effect on Fatigue Crack Propagation Using EBSD, FIB-DIC and FEM Methods. Engineering Fracture Mechanics. (Under review).

Song B., Xin R., Liao A., Yu W., Liu Q., 2105. Enhancing stretch formability of rolled Mg sheets by pre-inducing contraction twins and recrystallization annealing. Materials Science & Engineering A 627, 369–373

Walker K. The effect of stress ratio during crack propagation and fatigue for 2024-T3 and 7075-T6 aluminium. In: Rosenfeld M, ed. Effects of Environment and Complex Load History on Fatigue Life, ASTM STP 462. 1970, 1-4.

Wheeler O.E., 1972. Spectrum loading and crack growth. J. of Basic Eng. 94, 181-6

Xiaoping H., Moan T., Weicheng C., 2008. An engineering model of fatigue crack growth under variable amplitude loading. Int. Journal of Fatigue.

Yang, Q., Ghosh, A. K., 2006. Production of Ultrafine-Grain Microstructure in Mg Alloy by Alternate Biaxial Reverse Corrugation," Acta Mater., 54(19), 5147–5158.

Yuen B.K.C., Taheri F., 2006. Proposed modifications to the Wheeler retardation model for multiple overloading fatigue life prediction, International Journal of Fatigue 28, 1803-1819

Zheng J.,Powel B. E., 1997. A Method To Reduce The Scatter In Fatigue Crack Growth Rate Data. Fatigue Fract. Engng Mater. Struct. 20(9), 1341-1350.